Optics Letters

Effect of emitter orientation on the outcoupling efficiency of perovskite light-emitting diodes

CHEN ZOU* AND LIH Y. LIN

Department of Electrical and Computer Engineering, University of Washington, Seattle, Washington 98195, USA
**Corresponding author: chenzou@uw.edu*

Received 24 June 2020; revised 28 July 2020; accepted 28 July 2020; posted 29 July 2020 (Doc. ID 400814); published 24 August 2020

Metal halide perovskite light-emitting diodes (PeLEDs) have experienced a rapid advancement in the last several years with the external quantum efficiencies (EQEs) reaching over 20%, comparable to the state-of-the-art organic LEDs and quantum dot LEDs. The photoluminescence quantum yields of perovskite films have also been approaching 100%. Therefore, the next step to improving the EQE of PeLEDs should be focused on boosting light extraction. In this Letter, we demonstrate the emitter dipole orientation as a key parameter in determining the outcoupling efficiency of PeLEDs. We find that the $CsPbBr_3$ emitter has a slightly preferred orientation with the horizontal-to-vertical dipole ratio of 0.41:0.59, as compared to 0.33:0.67 in the isotropic case. A theoretical analysis predicts that a purely anisotropic perovskite emitter may result in a maximum EQE of 36%.

https://doi.org/10.1364/OL.400814

Metal halide perovskites have attracted intense interest recently due to their excellent properties, including high photoluminescence quantum yield (PLQY), facile bandgap tunability, and simple solution processability [1]. They have been widely used in a great variety of optoelectronic devices such as photovoltaics, photodetectors, light-emitting diodes (LEDs), and lasers [2–14]. Perovskite LEDs (PeLEDs) have gone through a rapid development, and the external quantum efficiencies (EQEs) have been improved from 0.76% [15] to over 20% [5,6,16–18] in the last several years. Besides, by appropriately passivating defects, the internal PLQYs of perovskite thin films have been approaching 100% [19–21]. However, the highest EQE that a PeLED can achieve is still limited by the light outcoupling efficiency [22]. Recent studies have shown that around 75–80% of generated power from perovskite films is trapped in PeLEDs due to the high refractive index ($n > 2$) of perovskite films, restricting the maximum outcoupling efficiency of PeLEDs to 20%–25% [5,23].

Presently, most research efforts are focused on analyzing and improving the optoelectronic properties of perovskite materials; there are few publications dealing with light outcoupling of PeLEDs [22–28]. If we retrospect the development histories of organic LEDs (OLEDs) and quantum dot LEDs (QLEDs), research is often concentrated on material exploration in the beginning. However, once the material development reaches a mature stage, more efforts are delved into the optimization of light extraction. [29] PeLEDs are expected to follow the same trajectory; therefore, the next step to optimizing PeLEDs should be focused on improving light outcoupling efficiency. In fact, there are already some outcoupling techniques successfully applied in PeLEDs. For examples, Zhang *et al.* fabricated PeLEDs on three-dimensional nanophotonic substrates to enhance light extraction [26]. Shen *et al.* integrated bioinspired moth eye nanostructures into a ZnO layer and achieved a record EQE of 28.2% among PeLEDs at that time [27]. However, these techniques usually require complicated fabrication procedures to produce photonic nanostructures. Engineering the optoelectronic properties of materials used in PeLEDs can provide more cost-effective approaches to increasing their EQEs. The investigation on the underlying physics of light outcoupling from PeLEDs is a necessary step toward this goal. Shi *et al.* have revealed the effects of the thickness and refractive index of perovskite films on light outcoupling from PeLEDs [23]. In this Letter, we demonstrate that the emitter orientation also plays an important role in light extraction from PeLEDs. In general, the EQE of a PeLED is determined by four individual factors [23,25]:

$$\mathrm{EQE} = \eta \mathrm{IQE} = \eta \gamma \eta_{S/T} q_{\mathrm{eff}}, \tag{1}$$

where η is the light outcoupling efficiency, and IQE is the internal quantum efficiency, which is the product of the charge injection balance (γ), the singlet/triplet capture ratio ($\eta_{S/T}$), and the effective radiative quantum yield (q_{eff}). Generally, the $\eta_{S/T}$ is close to unity for perovskite films; thus, we can usually neglect this item in the equation [23]. The effective radiative quantum yield is closely connected to the intrinsic quantum yield (q) of perovskite films; the relationship can be described as [30]

$$\frac{q_{\mathrm{eff}}}{q} = \frac{F}{qF + 1 - q}, \tag{2}$$

where F is the Purcell factor that describes how the cavity affects the dipole power generated inside the perovskite layer.

The charge injection balance can be well adjusted by selecting proper transport layers and tuning their thicknesses [31]. The effective quantum yield can be improved by passivating defects and confining bounded excitons [32]. Therefore, Eq. (1) shows that studying the limits of the light outcoupling

efficiency η is of great importance for achieving a high EQE. Figure 1(a) shows the device structure of the PeLED studied in this Letter. The device consists of a glass substrate covered with a 150 nm thick indium tin oxide (ITO) layer. A $CsPbBr_3$ layer with various thickness is sandwiched between a 30 nm poly-TPD layer (hole transport layer [HTL]) and a 40 nm TPBi (electron transport layer [ETL]). The functional layers between the bottom glass and top metal constitute the PeLED cavity. Figure 1(b) illustrates the coordinate system and definition of dipole orientations used in the following analysis. We adopt an optical simulation based on a classical dipole model to study the effect of the dipole orientation on the outcoupling efficiency of PeLEDs [33,34]. The emitting dipoles in perovskite films with random orientation can be treated as a superposition of p_x, p_y, and p_z dipoles. With respect to the substrate plane ($x-y$), we define p_x and p_y dipoles as being oriented horizontally, while p_z diploes are oriented vertically. If we choose the $x-z$ plane as the plane of incidence, p_y dipoles emit s-polarized light, whereas p_x and p_z dipoles are accounting for p-polarized emission [35]. The radiation of a dipole is strongest when it is perpendicular to the dipole orientation [36]. Therefore, p_z dipoles mainly emit light travelling with a large angle to the surface normal (z direction) [37]. Due to the total internal reflection (TIR), the generated light with a large emission angle can easily be trapped inside the functional layers (ITO, HTL, perovskite, ETL) and couple to evanescent waves at the ETL/metal interface, accounting for a low outcoupling efficiency for light emitted from p_z dipoles. Therefore, horizontally oriented p_x and p_y dipoles are preferred in terms of improving light extraction from PeLEDs. The ratio of the vertical dipoles to total dipoles is defined as Θ, and it is equal to 0.33 in the isotropic dipole case. We assume that the charge injection is well balances with $\gamma = 1$, and the intrinsic quantum yield $q = 0.9$, according to state-of-art PLQYs of perovskite films in reported literatures [19,21]. The refractive index of the $CsPbBr_3$ film is $\approx$2.2 near the emission wavelength [23]. The emission zone is assumed to be infinitely thin and locate at the middle of the perovskite layer.

Figure 1(c) shows the total optical power distribution diagram of PeLEDs (30 nm thick emitter) with isotropic dipole orientation ($\Theta = 0.33$). We can distinguish four optical channels of PeLEDs from left to right: direct emission, substrate mode, waveguide mode, and surface plasmon mode [22]. These four channels are separated by the in-plane wavevector k_{xy}. (1) Direct emission: $k_0 \cdot n_{\text{air}} \geq k_{xy} \geq 0$, where $k_0 = 2\pi/\lambda$ is the vacuum wave vector, and n_{air} is the refractive index of air. In this region, light outcouples into the air from PeLEDs. (2) Substrate mode: $k_0 \cdot n_{\text{sub}} \geq k_{xy} \geq k_0 \cdot n_{\text{air}}$, where n_{sub} is the refractive index of the substrate. In this region, light is trapped in the substrate due to the TIR at the substrate and air interface. (3) Waveguide mode: $k_0 \cdot n_{\text{eff}} \geq k_{xy} \geq k_0 \cdot n_{\text{sub}}$, where n_{eff} is the effective refractive index of the functional layers. In this region, light is trapped in functional layers because of the TIR at the ITO and substrate interface. (4) Surface plasmon mode: $k_{xy} \geq k_0 \cdot n_{\text{eff}}$. In this region, light couples to the top metal electrode in the form of evanescent waves. It is noticed that a large portion of optical power couples to two sharp waveguide modes (region 3) and one surface plasmon mode (region 4). Figure 1(d) shows the individual contributions from p_x, p_y, and p_z dipoles to the power dissipation spectra. Most of the optical power generated from p_z dipoles couples to surface plasmon and waveguide modes, consistent with the low outcoupling

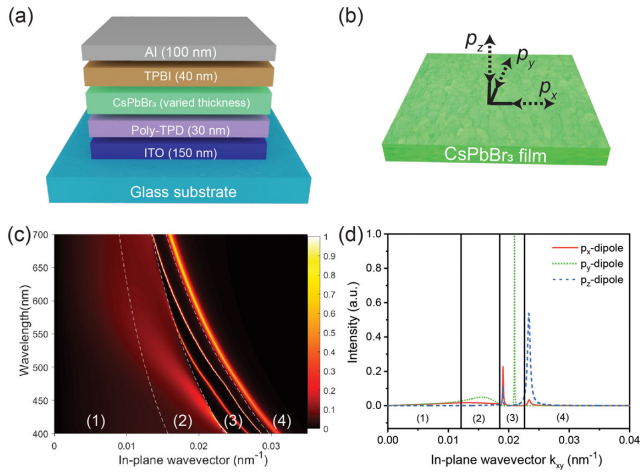

Fig. 1. (a) Schematic structure of the PeLED studied in this Letter. The thickness of the perovskite layer is varied. (b) Definition of dipole orientations. (c) Simulated power distribution diagram in PeLEDs (30 nm thick emitter) assuming isotropic emitter orientation. The white dashed lines divide the graph into four regions: (1) direction emission, (2) substrate mode, (3) waveguide mode, and (4) surface plasmon mode. (d) Power dissipation spectrum of p_x, p_y, and p_z dipoles at the emission wavelength of 523 nm.

efficiency for vertically oriented dipoles. In contrast, both horizontally oriented p_x and p_y dipoles have large contributions to the direct emission mode. The two distinct sharp peaks in region 3 correspond to p-polarized and s-polarized waveguide modes for p_x and p_y dipoles, respectively.

Figures 2(a) and 2(b) present the simulated power distribution into different optical modes of PeLEDs with various perovskite layer thicknesses for isotropic ($\Theta = 0.33$) and horizontal ($\Theta = 0$) dipole orientation, respectively. The nonradiative loss reflects the effective quantum yield q_{eff}, which is affected by the Purcell factor of a PeLED cavity [30]. The variation of the perovskite layer thickness greatly modifies the PeLED cavity length, accounting for the oscillating behaviors in direct emission. The power fraction of the waveguide mode shows oscillations as well, corresponding to constructive and destructive interference inside the micro-cavity. However, the coupling to surface plasmons is mainly determined by the distance from the emitting dipole location to the metal electrode. Therefore, the power fraction of the surface plasmon mode shows a declining trend as the perovskite layer thickness increases. As only vertically oriented dipoles mainly contribute to the surface plasmon mode, PeLEDs with horizontal dipole orientation show a much smaller power fraction of the surface plasmon mode. The outcoupling efficiency of light from horizontally aligned dipoles is higher compared to vertical ones for most perovskite layer thicknesses. The exceptional case happens at the thickness where the outcoupling efficiency is close to minimum. This is due to different phase shifts for the reflections at the ETL/cathode interface for vertical and horizontal dipole radiation, which causes the corresponding maxima and minima for direct emission are displaced [36].

Angular p-polarized photoluminescence (PL) measurements can be used to determine the dipole orientation of perovskite films [29,38]. Figure 3(a) schematically illustrates the experimental setup. A 40 nm thick $CsPbBr_3$ film deposited on a glass substrate is excited by a continuous-wave laser with a wavelength

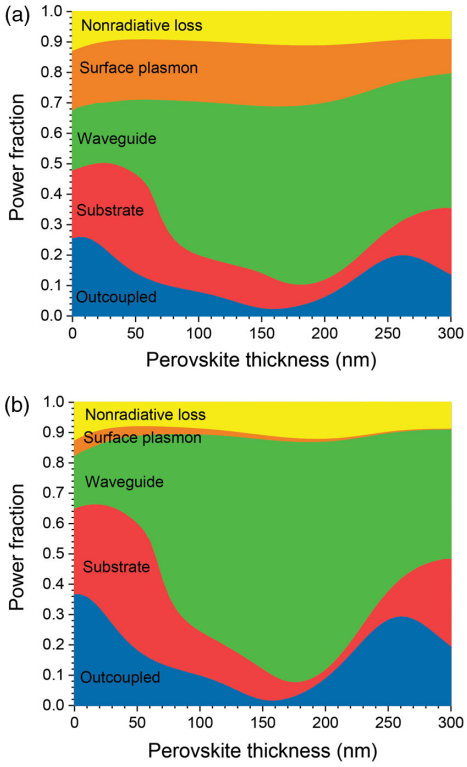

Fig. 2. Power distribution into different optical modes of PeLEDs with various perovskite layer thicknesses for (a) isotropic dipole orientation ($\Theta = 0.33$) and (b) horizontal dipole orientation ($\Theta = 0$).

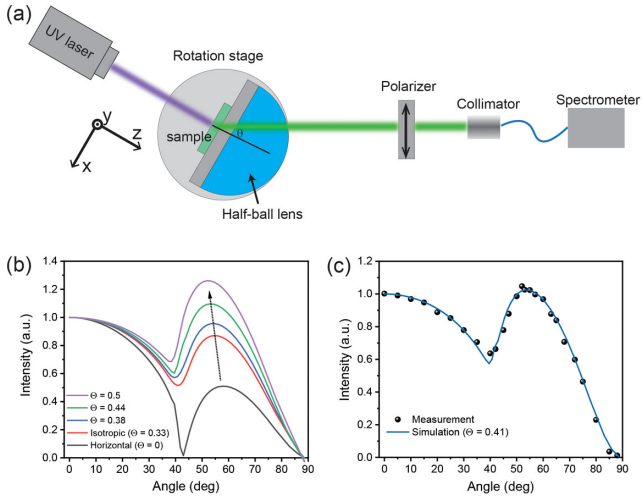

Fig. 3. (a) Schematic experimental setup for measuring the dipole orientation of perovskite films. (b) Simulated p-polarized PL intensity as a function of the emission angle. (c) Measured data and the fitting curve ($\Theta = 0.41$).

of 405 nm. The excitation spot size is less than 1 mm^2. To extract the light trapped in the substrate, a glass half-ball lens is attached to the substrate with index-matching fluid (IMF, $n = 1.52$). The whole sample is placed at the center of a rotation stage, which can be rotated to various angles. The $x-y-z$ coordinate is annotated for the sample rotated to the angle θ. The angular light emissions go through a linear polarizer with a vertical polarization axis (annotated inside the polarizer) and then get collected by a fiber-coupled spectrometer with a collimator. The light emitted from p_y dipoles is s-polarized (perpendicular to $x-z$ plane), which will be blocked by the polarizer filter. The angular PL is only contributed by p-polarized emission from horizontally oriented p_x dipoles and vertically oriented p_z dipoles. We simulated the angular p-polarized PL intensity profiles assuming different dipole orientations of perovskite films; the results are shown in Fig. 3(b). Because the optical power in the substrate mode can be extracted by the attached half-ball lens, there are PL intensity peaks emerging at the angles greater than approximately 42° (the TIR angle at the substrate and air interface). As the vertical dipole ratio (Θ) increases, the intensity of this peak also increases. This is because, for this sample without the metal electrode, the vertical dipoles radiate mostly into the substrate mode, while the horizontal ones mainly outcouple to the air. The PL intensity peaks at angles great than 42° can be used to quantify the Θ value. By fitting measured experimental data (solid circles) in Fig. 3(c), we extract the value of Θ to be 0.41. The slightly preferred vertical dipole orientation in $CsPbBr_3$ films is consistent with reported literatures, [25,28,39,40] and it may be caused by induced vertical alignment of dipoles at the perovskite/substrate interface due to localized electrostatic surface charges [28,39]. However, the Θ value is also highly dependent on film morphology, crystal orientation, electronic transfer, and dielectric environment [5,28,39–41]. By depositing a Al_2O_3 layer on top of perovskite nanocrystal films, Jurow *et al.* could counterbalance the influence of the substrate and decrease the transition dipole to surface angle by more than 50% to only 14° [28]. The feasibility to control the dipole orientation of perovskite films provides great potential for achieving high-efficiency PeLEDs.

To present potential device efficiencies by controlling emissive transition dipole moments, we investigated the dependence of the EQE on the dipole orientation and perovskite layer thickness (assuming $\gamma = 1$, $q = 0.9$). Figure 4 shows that both factors significantly influence the EQE. For PeLEDs with various perovskite layer thicknesses, the EQE increases as the dipole orientation become more horizontal (Θ decreases). This indicates further improvement of PeLEDs should be feasible through designing perovskite materials with more horizontally oriented dipoles. The optimal thickness of the $CsPbBr_3$ layer in PeLEDs is 10–15 nm in the case of $\Theta = 0.41$. However, even for a 30 nm thick $CsPbBr_3$ layer ($\Theta = 0.41$), the EQE can keep at ~20%. Such thickness is commonly used in PeLEDs because a perovskite layer that is too thin leads to poor coverage and shorting problems, and a perovskite layer that is too thick leads to loss of electron-hole pairs for radiative recombination during the charge transport process. In our simulation, the maximum EQE that PeLEDs can achieve is about 36% with a horizontal dipole orientation ($\Theta = 0$). Considering the current record efficiency of 21.6% among PeLEDs without outcoupling nanostructures [42], we believe there is still much room for the performance improvement of PeLEDs.

In summary, we have investigated the effect of the dipole orientation on the outcoupling efficiency of PeLEDs through optical simulations. We show that horizontally oriented dipoles are preferred over vertically oriented dipoles in terms of improving light extraction. A perovskite emitter with a horizontal transition dipole moment can lead to a potential maximum EQE of 36% considering an IQE of 90%, well beyond the limits

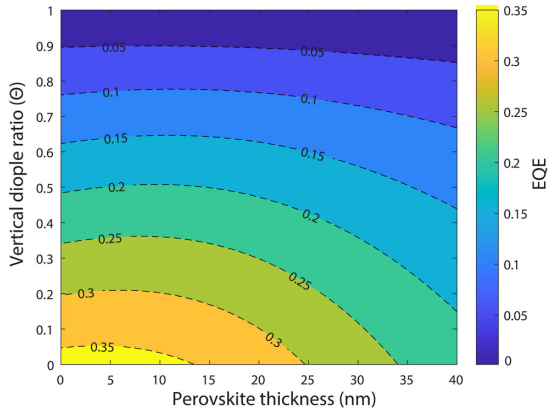

Fig. 4. Contour plot of the simulated EQE as a function of the perovskite layer thickness and vertical dipole ratio (Θ). The black dashed lines represent the contour lines of the EQEs.

of isotropic light sources. By performing angular p-polarized PL measurements, we find the dipole orientation in $CsPbBr_3$ films is more vertically oriented, which is not very favorable in terms of light extraction. Further control of the dipole orientation of perovskite films by engineering film morphology, crystal orientation, and interfacial interactions holds great promise for the significant advancement of PeLED performance.

Funding. National Science Foundation (ECCS-1807397).

Disclosures. The authors declare no conflicts of interest.

REFERENCES

1. B. R. Sutherland and E. H. Sargent, Nat. Photonics **10**, 295 (2016).
2. A. Swarnkar, A. R. Marshall, E. M. Sanehira, B. D. Chernomordik, D. T. Moore, J. A. Christians, T. Chakrabarti, and J. M. Luther, Science **354**, 92 (2016).
3. H. Wang, P. Zhang, and Z. Zang, Appl. Phys. Lett. **116**, 162103 (2020).
4. C. Zou, J. Zheng, C. Chang, A. Majumdar, and L. Y. Lin, Adv. Opt. Mater. **7**, 1900558 (2019).
5. Y. Cao, N. Wang, H. Tian, J. Guo, Y. Wei, H. Chen, Y. Miao, W. Zou, K. Pan, Y. He, H. Cao, Y. Ke, M. Xu, Y. Wang, M. Yang, K. Du, Z. Fu, D. Kong, D. Dai, Y. Jin, G. Li, H. Li, Q. Peng, J. Wang, and W. Huang, Nature **562**, 249 (2018).
6. K. Lin, J. Xing, L. N. Quan, F. P. G. de Arquer, X. Gong, J. Lu, L. Xie, W. Zhao, D. Zhang, C. Yan, W. Li, X. Liu, Y. Lu, J. Kirman, E. H. Sargent, Q. Xiong, and Z. Wei, Nature **562**, 245 (2018).
7. C. Zou, Y. Liu, D. S. Ginger, and L. Y. Lin, ACS Nano **14**, 6076 (2020).
8. D. Yan, S. Zhao, H. Wang, and Z. Zang, Photonics Res. **8**, 1086 (2020).
9. G. Xing, B. Wu, X. Wu, M. Li, B. Du, Q. Wei, J. Guo, E. K. Yeow, T. C. Sum, and W. Huang, Nat. Commun. **8**, 14558 (2017).
10. C.-Y. Huang, C. Zou, C. Mao, K. L. Corp, Y.-C. Yao, Y.-J. Lee, C. W. Schlenker, A. K. Y. Jen, and L. Y. Lin, ACS Photonics **4**, 2281 (2017).
11. G. Xing, N. Mathews, S. S. Lim, N. Yantara, X. Liu, D. Sabba, M. Gratzel, S. Mhaisalkar, and T. C. Sum, Nat. Mater. **13**, 476 (2014).
12. G. Xing, M. H. Kumar, W. K. Chong, X. Liu, Y. Cai, H. Ding, M. Asta, M. Gratzel, S. Mhaisalkar, N. Mathews, and T. C. Sum, Adv. Mater. **28**, 8191 (2016).
13. H. Guan, S. Zhao, H. Wang, D. Yan, M. Wang, and Z. Zang, Nano Energy **67**, 104279 (2020).
14. S. Zhao, Y. Zhang, and Z. Zang, Chem. Commun. **56**, 5811 (2020).
15. Z. K. Tan, R. S. Moghaddam, M. L. Lai, P. Docampo, R. Higler, F. Deschler, M. Price, A. Sadhanala, L. M. Pazos, D. Credgington, F. Hanusch, T. Bein, H. J. Snaith, and R. H. Friend, Nat. Nanotechnol. **9**, 687 (2014).
16. W. Xu, Q. Hu, S. Bai, C. Bao, Y. Miao, Z. Yuan, T. Borzda, A. J. Barker, E. Tyukalova, and Z. Hu, Nat. Photonics **13**, 418 (2019).
17. T. Chiba, Y. Hayashi, H. Ebe, K. Hoshi, J. Sato, S. Sato, Y.-J. Pu, S. Ohisa, and J. Kido, Nat. Photonics **12**, 681 (2018).
18. B. Zhao, S. Bai, V. Kim, R. Lamboll, R. Shivanna, F. Auras, J. M. Richter, L. Yang, L. Dai, M. Alsari, X.-J. She, L. Liang, J. Zhang, S. Lilliu, P. Gao, H. J. Snaith, J. Wang, N. C. Greenham, R. H. Friend, and D. Di, Nat. Photonics **12**, 783 (2018).
19. I. L. Braly, D. W. DeQuilettes, L. M. Pazos-Outón, S. Burke, M. E. Ziffer, D. S. Ginger, and H. W. Hillhouse, Nat. Photonics **12**, 355 (2018).
20. X. Zheng, S. Yuan, J. Liu, J. Yin, F. Yuan, W.-S. Shen, K. Yao, M. Wei, C. Zhou, K. Song, B.-B. Zhang, Y. Lin, M. N. Hedhili, N. Wehbe, Y. Han, H.-T. Sun, Z.-H. Lu, T. D. Anthopoulos, O. F. Mohammed, E. H. Sargent, L.-S. Liao, and O. M. Bakr, ACS Energy Lett. **5**, 793 (2020).
21. M. Abdi-Jalebi, Z. Andaji-Garmaroudi, S. Cacovich, C. Stavrakas, B. Philippe, J. M. Richter, M. Alsari, E. P. Booker, E. M. Hutter, A. J. Pearson, S. Lilliu, T. J. Savenije, H. Rensmo, G. Divitini, C. Ducati, R. H. Friend, and S. D. Stranks, Nature **555**, 497 (2018).
22. L. Zhao, K. M. Lee, K. Roh, S. U. Z. Khan, and B. P. Rand, Adv. Mater. **31**, 1805836 (2019).
23. X.-B. Shi, Y. Liu, Z. Yuan, X.-K. Liu, Y. Miao, J. Wang, S. Lenk, S. Reineke, and F. Gao, Adv. Opt. Mater. **6**, 1800667 (2018).
24. S.-S. Meng, Y.-Q. Li, and J.-X. Tang, Org. Electron. **61**, 351 (2018).
25. T. Morgenstern, C. Lampe, T. Naujoks, M. Jurow, Y. Liu, A. S. Urban, and W. Brütting, J. Lumin. **220**, 116939 (2020).
26. Q. Zhang, M. M. Tavakoli, L. Gu, D. Zhang, L. Tang, Y. Gao, J. Guo, Y. Lin, S. F. Leung, S. Poddar, Y. Fu, and Z. Fan, Nat. Commun. **10**, 727 (2019).
27. Y. Shen, L. P. Cheng, Y. Q. Li, W. Li, J. D. Chen, S. T. Lee, and J. X. Tang, Adv. Mater. **31**, 1970174 (2019).
28. M. J. Jurow, T. Morgenstern, C. Eisler, J. Kang, E. Penzo, M. Do, M. Engelmayer, W. T. Osowiecki, Y. Bekenstein, C. Tassone, L. W. Wang, A. P. Alivisatos, W. Brutting, and Y. Liu, Nano Lett. **19**, 2489 (2019).
29. S.-Y. Kim, W.-I. Jeong, C. Mayr, Y.-S. Park, K.-H. Kim, J.-H. Lee, C.-K. Moon, W. Brütting, and J.-J. Kim, Adv. Funct. Mater. **23**, 3896 (2013).
30. R. Zhu, Z. Luo, and S. T. Wu, Opt. Express **22**, A1783 (2014).
31. A. Fakharuddin, W. Qiu, G. Croes, A. Devižis, R. Gegevičius, A. Vakhnin, C. Rolin, J. Genoe, R. Gehlhaar, A. Kadashchuk, V. Gulbinas, and P. Heremans, Adv. Funct. Mater. **29**, 1904101 (2019).
32. X. Yang, X. Zhang, J. Deng, Z. Chu, Q. Jiang, J. Meng, P. Wang, L. Zhang, Z. Yin, and J. You, Nat. Commun. **9**, 570 (2018).
33. R. R. Chance, A. Prock, and R. Silbey, J. Chem. Phys. **60**, 2744 (1974).
34. M. H. Lu and J. C. Sturm, Appl. Phys. Lett. **78**, 1927 (2001).
35. W. Brütting, J. Frischeisen, T. D. Schmidt, B. J. Scholz, and C. Mayr, Phys. Status Solidi A **210**, 44 (2013).
36. T. D. Schmidt, T. Lampe, D. Sylvinson, M. R. P. I. Djurovich, M. E. Thompson, and W. Brütting, Phys. Rev. Appl. **8**, 037001 (2017).
37. J. Frischeisen, D. Yokoyama, A. Endo, C. Adachi, and W. Brütting, Org. Electron. **12**, 809 (2011).
38. J. Frischeisen, D. Yokoyama, C. Adachi, and W. Brütting, Appl. Phys. Lett. **96**, 073302 (2010).
39. M. J. Jurow, T. Lampe, E. Penzo, J. Kang, M. A. Koc, T. Zechel, Z. Nett, M. Brady, L. W. Wang, A. P. Alivisatos, S. Cabrini, W. Brutting, and Y. Liu, Nano Lett. **17**, 4534 (2017).
40. G. Walters, L. Haeberle, R. Quintero-Bermudez, J. Brodeur, S. Kena-Cohen, and E. H. Sargent, J. Phys. Chem. Lett. **11**, 3458 (2020).
41. X. Zhang, G. Wu, W. Fu, M. Qin, W. Yang, J. Yan, Z. Zhang, X. Lu, and H. Chen, Adv. Energy. Mater. **8**, 1702498 (2018).
42. W. Xu, Q. Hu, S. Bai, C. Bao, Y. Miao, Z. Yuan, T. Borzda, A. J. Barker, E. Tyukalova, Z. Hu, M. Kawecki, H. Wang, Z. Yan, X. Liu, X. Shi, K. Uvdal, M. Fahlman, W. Zhang, M. Duchamp, J.-M. Liu, A. Petrozza, J. Wang, L.-M. Liu, W. Huang, and F. Gao, Nat. Photonics **13**, 418 (2019).